A nucleoid-associated protein is involved in the emergence of antibiotic resistance by promoting the frequent exchange of the replicative DNA polymerase in *M. smegmatis*

Wei L. Ng [a] and E. Hesper Rego[1] [a]

Affiliations

[a] Department of Microbial Pathogenesis, Yale University School of Medicine, New Haven, CT 06519

[1]To whom correspondence should be addressed: hesper.rego@yale.edu

SUMMARY

Antibiotic resistance in *M. tuberculosis* exclusively originates from chromosomal mutations, either during normal DNA replication or under stress, when the expression of error-prone DNA polymerases increases to repair damaged DNA. To bypass DNA lesions and catalyze error-prone DNA synthesis, translesion polymerases must be able to access the DNA, temporarily replacing the high-fidelity replicative polymerase. The mechanisms that govern polymerase exchange are not well understood, especially in mycobacteria. Here, using a suite of quantitative fluorescence imaging techniques, we discover that, as in other bacterial species, in *M. smegmatis,* the replicative polymerase, DnaE1, exchanges at a timescale much faster than that of DNA replication. Interestingly, this fast exchange rate depends on an actinobacteria-specific nucleoid-associated protein (NAP), Lsr2. In cells missing *lsr2*, DnaE1 exchanges less frequently, and the chromosome is replicated more faithfully. Additionally, in conditions that damage DNA, cells lacking *lsr2* load the complex needed to bypass DNA lesions less effectively

and, consistently, replicate with higher fidelity but exhibit growth defects. Together, our results show that Lsr2 promotes dynamic flexibility of the mycobacterial replisome, which is critical for robust cell growth and lesion repair in conditions that damage DNA.

Importance. Unlike many other pathogens, *M. tuberculosis* has limited ability for horizontal gene transfer, a major mechanism for developing antibiotic resistance. Thus, the mechanisms that facilitate chromosomal mutagenesis are of particular importance in mycobacteria. Here, we show that Lsr2, a nucleoid-associated protein, has a novel role in DNA replication and mutagenesis in the model mycobacterium *M. smegmatis*. We find that Lsr2 promotes the fast exchange rate of the replicative DNA polymerase, DnaE1, at the replication fork and is important for the effective loading of the DnaE2-ImuA'-ImuB translesion complex. Without *lsr2*, *M. smegmatis* replicates its chromosome more faithfully and acquires resistance to rifampin at a lower rate, but at the cost of impaired survival to DNA damaging agents. Together, our work establishes Lsr2 as a potential factor in the emergence of mycobacterial antibiotic resistance.

INTRODUCTION

DNA replication and repair are fundamental to bacterial evolution. The function of DNA replication and repair pathways are key determinants of the balance between genetic stability and mutability. To establish this balance, bacteria encode and regulate numerous DNA polymerases with specialized functions in different conditions (1). Importantly, the emergence of antibiotic resistance in the major human pathogen *M. tuberculosis* is mainly driven by chromosomal mutagenesis, as *M. tuberculosis* has no ability for horizontal gene transfer (2, 3). Thus, the mechanisms regulating polymerase expression and activity are of particular importance for mycobacterial evolution.

48 In mycobacteria, the fidelity of chromosome replication is established by the major
49 replicative polymerase DnaE1, which possesses endogenous proofreading activity (4). In
50 addition to DnaE1, mycobacteria encode a suite of other polymerases with specialized repair
51 functions that are only expressed under certain conditions, such as oxidative or DNA-damaging
52 stress (5-7). For example, the mycobacterial specialist polymerases DinB1, DinB2, DinB3, and
53 DnaE2 are induced under different conditions and have varying repair activities and mutational
54 signatures (5-10). Of particular importance is the error-prone polymerase DnaE2. It and its
55 accessory proteins ImuA' and ImuB – collectively referred to as the 'mutasome' – are highly
56 expressed in conditions that damage DNA and are the primary drivers of stress-induced
57 mutagenesis *in vitro* and potentially *in vivo* (5, 6, 11). In general, however, the mechanisms that
58 facilitate switching between polymerases at the site of repair are not well understood, especially
59 in mycobacteria (12).

60 It is known that in non-DNA damaging conditions, in *E. coli*, components within the large
61 multi-protein complex that replicates DNA (the replisome) exchange rapidly, likely when
62 encountering DNA-protein obstacles. More specifically, fluorescence recovery after
63 photobleaching (FRAP) and single molecule studies have revealed that, despite being highly
64 processive *in vitro*, replisome components are highly dynamic within the cell (13). For example,
65 at room temperature, the alpha subunit of Pol III in *E. coli* exchanges with the cytoplasmic pool
66 at a time scale of approximately 4 seconds, suggesting that subunits are constantly being
67 replaced during the 150 minutes it takes to replicate the chromosome at this temperature (13).
68 These data underlie the notion that the replisome is dynamic and flexible, allowing new subunits
69 the opportunity to exchange frequently and suggest that protein obstacles influence the
70 exchange rate of replisome components.

71 Mycobacteria differ from model bacteria like *E. coli* in several ways. Most notable is their
72 slow growth and long doubling times. Pathogenic mycobacteria, like *M. tuberculosis* and *M.*

73 *leprae*, are notorious for their long doubling times, which can vary from 18 hours to several
74 weeks. Even so-called fast growers like *M. smegmatis* double on the hour-long timescale
75 compared to the minute-long timescale of commonly studied organisms like *E. coli*. Intriguingly,
76 the duration of chromosomal replication at least partially scales with growth rate: *M. smegmatis*
77 exhibits a longer duration of chromosome replication than *E. coli* (~100-150 minutes vs ~41
78 minutes, respectively) despite the ability of DnaE1 to polymerize DNA at a faster rate than *E.*
79 *coli* Pol IIIα *in vitro* (4, 14, 15).

80 These observations led us to wonder if components within the replisome exchange at a
81 different timescale in mycobacteria than in faster-growing bacteria. Using various fluorescence
82 imaging techniques, we find that, as in *E. coli*, the replicative polymerase is exchanged rapidly
83 in *M. smegmatis*. Surprisingly, this fast exchange rate is, in part, mediated by an actinobacteria-
84 specific DNA-binding protein Lsr2, as DnaE1 is exchanged more slowly in cells missing *lsr2*.
85 Interestingly, when the DNA is damaged, ImuB, a key scaffolding protein that recruits the error-
86 prone polymerase into an active complex, is exchanged more rapidly, suggesting ineffective
87 loading of the mutasome. Consistently, loss of *lsr2* results in growth defects in conditions that
88 damage DNA, and reduced mutagenesis. Overall, our data deepen our understanding of DNA
89 metabolism in mycobacteria and provide another unexpected layer to the mechanisms
90 mycobacteria use to mutate and acquire drug resistance.

91 **RESULTS**

92 **The mycobacterial replisome is highly dynamic**

93 To investigate the dynamics of DnaE1, we created a strain expressing DnaE1-mScarlet
94 from its native promoter. A similar fusion encodes functional DnaE1 (16). To verify that DnaE1-
95 mScarlet reports on the localization of the replisome, we performed time-lapse microscopy and
96 analyzed fluorescence distributions as a function of both cell length and cell cycle (**Fig. 1A, B**).

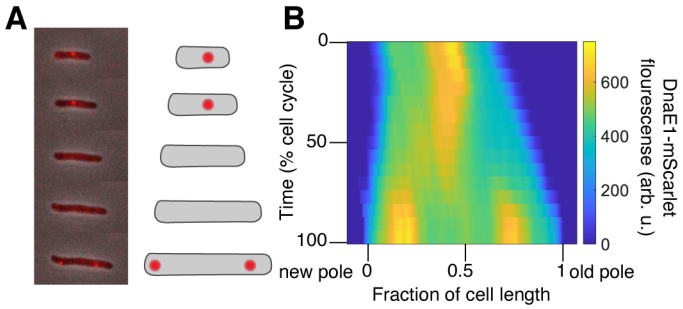

Figure 1. DnaE1 localization over time in *M. smegmatis.* (A) A representative cell expressing DnaE1-mScarlet from its native promoter is imaged over time with both phase and fluorescence microscopy. Fluorescent spots appear at mid-cell, disappear, and then re-appear at roughly one- and three-quarters positions at the end of one cell cycle/beginning of another. **(B)** To quantify fluorescence probability distributions over time and space, we constructed kymographs by averaging individual distributions that were normalized to cell cycle time and length (N=43).

Consistent with the reported placement of the replisome in mycobacteria, DnaE1 localizes at the approximately mid-cell before disappearing, presumably after DNA replication has been completed (16). Towards the end of the cell cycle, DnaE1 reappears at one- and three-quarter positions to initiate replication in newly synthesized sister chromosomes (**Fig. 1A, B**). These data show that DnaE1-mScarlet is reporting on the localization of the replisome in *M. smegmatis*.

To test the exchange rate of DnaE1, we took the same approach as Beattie, TR *et al* and used FRAP to measure the dynamics of recovery of DnaE1 in cells (13). Fast recovery of fluorophores into a bleached spot indicates fast dissociation of bleached molecules. Conversely, slow, or incomplete recovery of non-bleached fluorophores indicates slow dissociation of bleached molecules, and a stably associated complex. To account for differences in the degree of bleaching per cell, we normalized the fluorescence intensity after bleaching to zero, and the final intensity to the maximum recovery we expected based on the percentage of fluorophores bleached. We fit the data to a diffusion exchange reaction and calculated both the timescale of recovery, reflecting the dissociation time of bound subunits, and the maximum recovery, reflecting the mobile fraction of proteins. Imaging was done in the same conditions as above, in which we measured the duration of chromosomal replication to be approximately 100 minutes

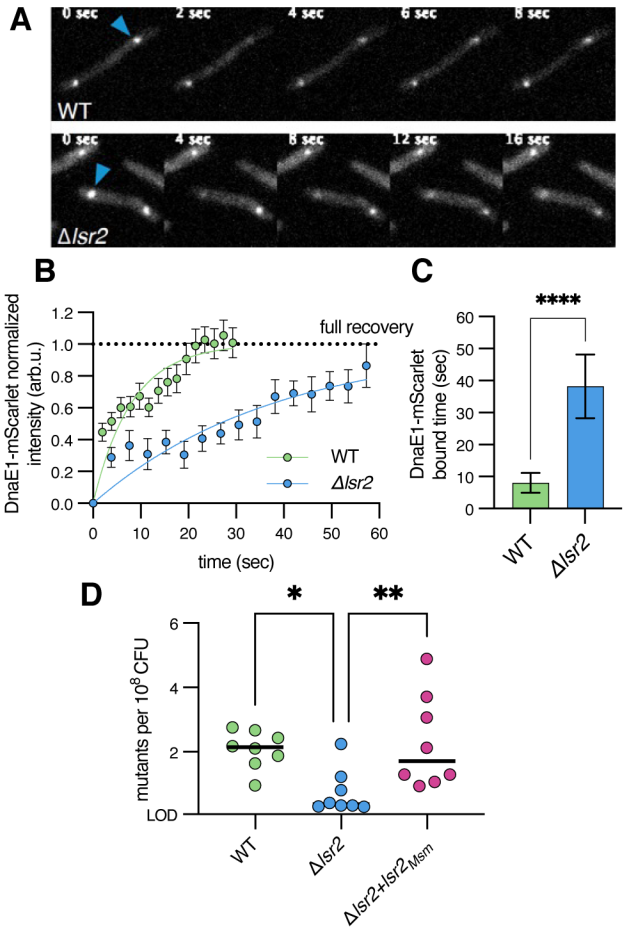

Figure 2. The replicative polymerase is highly dynamic, which is in part mediated by Lsr2. (A) Representative time sequence of FRAP of DnaE1-mScarlet in WT (top) and Δ*lsr2* (bottom) imaged at 2 and 4-second intervals, respectively. Blue arrow indicates the location of the focus targeted for bleaching. **(B)** Fluorescence recovery curves for DnaE1-mScarlet (N=21 for WT, 12 for Δ*lsr2*). Solid lines show a one-phase exponential association fit to the data. Individual points show the mean±SEM of fluorescence intensity after bleach correction. Dashed line represents the estimated maximum possible fluorescence recovery. **(C)** DnaE1-mScarlet bound times (mean±SD) obtained from one-phase exponential association fits in panel B for both WT and Δ*lsr2* for DnaE1. (****), p<0.0001 by unpaired t-test. (**D**) Frequency of spontaneous rifampin-resistant mutants per 10^8 cfu. LOD refers to the limit of detection. *lsr2* complements were expressed from the native *lsr2* promoter on a phage integrative plasmid. p-values were obtained by one-way ANOVA. (*), p<0.0021 (**), p<0.0002.

114 based on the time between the appearance and disappearance of DnaE1 (**Fig. 1B, S2B**). We

115 found that, as in *E. coli*, DnaE1 exchanged quickly and nearly completely with a timescale of

116 approximately 8 +/- 3 seconds (mean±SD) (**Fig. 2A-C**). These data are consistent with the

117 model that has emerged in *E. coli,* which suggests that the replisome constantly encounters

118 obstacles that promote the exchange of individual subunits with the cytoplasmic pool.

119 **Lsr2 promotes the frequent exchange of DnaE1**

120 In bacteria, nucleoid-associated proteins (NAPS) are important for bacterial
121 chromosome organization and influence replication, transcription, and cell cycle regulation
122 either directly or indirectly. Lsr2 is one of the most well-studied NAPs in mycobacteria. Lsr2 is
123 conserved across mycobacteria and related actinomycetes (17-21). Like H-NS in *E. coli*, Lsr2
124 primarily binds AT-rich regions of DNA and functions as a global transcriptional repressor (18).
125 Notably, *in vitro* studies show that Lsr2 binding interferes with transcription, inhibits
126 topoisomerase I-dependent supercoil relaxation, and protects DNA from DNase I digestion and
127 H_2O_2-mediated degradation (17). Loss of *lsr2* is associated with a wide range of different
128 phenotypes in mycobacteria, including altered cell cycle timing and growth defects upon
129 entering/exiting hypoxic conditions and when exposed to oxidative stress and various antibiotics
130 (17, 22-25). Lsr2 is also involved in resistance against phage infection, protection against
131 reactive oxygen intermediates during macrophage infection, and cells missing *lsr2* show
132 reduced virulence in various hosts, including mice (20, 22, 23, 26).

133 ChIP-seq data show an abundance of Lsr2 binding sites across the chromosome, and
134 consistent with this, Lsr2 decorates the entire nucleoid in discrete and highly dynamic puncta
135 (24). Interestingly, the major Lsr2 foci are localized near, but not co-localized with, the
136 replisome. We verified this localization pattern in our hands by creating strains that express
137 Lsr2-mScarlet and DnaE1-mGFPmut3. Consistent with prior reports, Lsr2 and DnaE1 exhibit
138 distinct localizations, and although Lsr2 localizes nearby DnaE1 at certain times in the cell
139 cycle, Lsr2 does not co-localize with DnaE1 despite Lsr2's abundance throughout nucleoid (**Fig.
140 S1**).

141 Given the importance of Lsr2 to mycobacteria physiology and its localization, we
142 wondered if deletion of *lsr2* would influence replisome exchange dynamics. To that end, we

143 generated an *lsr2* deletion strain expressing DnaE1-mScarlet. Consistent with prior findings
144 using a DnaN reporter, we find that DnaE1 fluorescence disappears from the mid-cell region
145 faster in cells missing *lsr2*, suggesting that DNA replication is faster by approximately 20% (**Fig.**
146 **S2A, B**) (25). Next, as before, we measured the rate of DnaE1 recovery in *Δlsr2* cells using
147 FRAP (**Fig. 2A**). We observed a much longer recovery time (38 +/- 10 seconds) compared to
148 wild type cells (**Fig. 2B,C**). These data suggest that DnaE1 remains associated with the
149 replisome for longer in cells missing *lsr2*. Alternatively, a longer recovery time in the *lsr2* mutant
150 could be due to reduced DnaE1 access to the replisome (e.g.*,* due to increased access by other
151 polymerases to the replisome). However, reduced access by DnaE1, an essential polymerase in
152 *M. smegmatis*, would likely result in a growth rate difference in the mutant, which we and others
153 do not observe (**Fig. S2C**) (25). Likewise, reduced access by DnaE1 would also increase basal
154 mutation rates, as this polymerase is responsible for faithful chromosome replication in standard
155 laboratory medium (4). Instead, we observe that that Δ*lsr2* cells mutate at decreased frequency
156 as measured by spontaneous resistance to rifampin (**Fig. 2D**), further supporting the notion of
157 increased stability of DnaE1 in Δ*lsr2.* Taken together, these data show that Lsr2 promotes the
158 rapid exchange of DnaE1. In its absence, DnaE1 is more stably associated, and cells replicate
159 their chromosome more quickly and more faithfully.

160

161 **Lrs2 is important for the acquisition of mutations by promoting the stable formation of**
162 **the mutasome**

163 We next considered if Lsr2 also affects polymerase exchange in conditions that elevate
164 the expression of the error-prone polymerase DnaE2 and its associated complex. To test this,
165 we created strains carrying fluorescent proteins fusions to ImuA', ImuB, and DnaE2 integrated
166 either at a phage site (*imuA'* and *imuB* in Δ*imuAB*) or the chromosomal locus (*dnae2*). When

167 exposed to UV light, these strains acquired resistance to rifampin at a similar rate as wild type,
168 showing that the fusion proteins retain the ability to repair damaged DNA (**Fig. S3**) (27).

169 ImuB recruits ImuA' and DnaE2 into an active complex by binding to the β-clamp subunit
170 of the replisome. ImuA' and DnaE2 bind ImuB but not the β-clamp, and therefore require ImuB
171 to associate with the replisome and catalyze mutations (8, 11, 27, 28). Despite being co-
172 transcribed, ImuA'-mScarlet and mScarlet-ImuB had dramatically different fluorescence
173 intensities: ImuA'-mScarlet was barely detectable above background fluorescence levels, while
174 mScarlet-ImuB was brightly fluorescent (**Fig. S4A,B**). Thus, cellular levels of ImuA' may be
175 much lower than ImuB, implying that additional post-transcriptional mechanisms exist (e.g.
176 translation regulation or proteolysis) to limit ImuA' abundance. Alternatively, mScarlet may be
177 cleaved off the ImuA'-mScarlet translational fusion and targeted for degradation. However,
178 consistent with the low abundance of ImuA', we also observed very low fluorescence of DnaE2-
179 mGFPmut3 (**Fig. S4C**). Others have reported similar results using N-terminal fusions (27).
180 These data suggest that as in *E. coli,* the translesion polymerase abundance may be tightly
181 regulated post-transcriptionally (29). Further, these data suggest that one limiting factor in
182 forming an active mutasome complex may be the low cellular concentrations of ImuA' and/or
183 DnaE2.

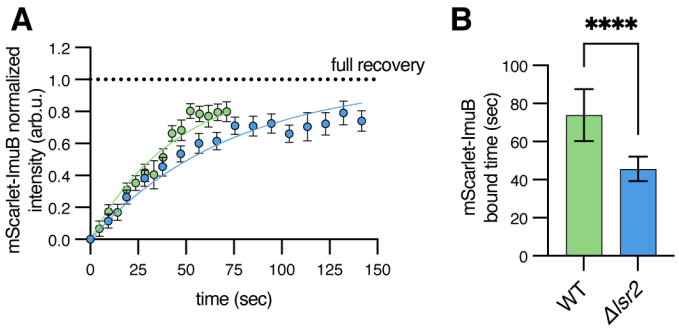

Figure 3. Lsr2 mediates stable loading of ImuB. Cells expressing mScalet-ImuB were treated with 1.56ng/ml mitomycin C for 4 hours before forming FRAP. **(A)** Fluorescence recovery curves for mScarlet-ImuB (N=13 for WT, 10 for Δ*lsr2*). Solid lines show a one-phase exponential association fit to the data. Individual points show the mean±SEM of fluorescence intensity after bleach correction. Dashed line represents the estimated maximum possible fluorescence recovery. **(B)** Bound times (mean±SD) obtained from one-phase exponential association fits from panel A. $p<0.0001$ by unpaired t-test.

184 Due to the dim fluorescence of ImuA' and DnaE2, it was difficult to draw conclusions
185 about their localization or dynamics in cells with or without *lsr2*. Thus, we decided to determine
186 the exchange rate of ImuB. We treated cells with a low concentration of mitomycin (MMC) to
187 induce expression of ImuB and, as before, performed FRAP. In wild type cells, ImuB displayed
188 a much longer timescale of exchange (74 +/- 14 seconds) compared to DnaE1, suggesting
189 ImuB remains associated with the β-clamp for a longer time (**Fig. 3A,B**). The long bound time of
190 ImuB is consistent with the need to recruit low-abundance proteins ImuA' and/or DnaE2. In cells
191 missing *lsr2*, ImuB exchanged more quickly (46 +/- 6 seconds) than in wild type, at a rate similar
192 to DnaE1-mScarlet (**Fig. 2C**). Thus, as ImuB and DnaE1 both bind the β -clamp, these data
193 suggest that the mutasome complex is less stably associated in cells missing *lsr2*, possibly due
194 to the increased stability of DnaE1.

195 To further test this hypothesis, we reasoned that Δ*lsr2* would phenocopy cells defective
196 in mutasome expression or stability. *M. smegmatis* and *M. tuberculosis* missing ImuA' and ImuB
197 are more sensitive to MMC treatment and are less likely to mutate when exposed to DNA-
198 damaging agents like ultraviolet light (**Fig. S3A**) (11, 27). Thus, we hypothesized that cells
199 missing *lsr2* would be altered in these key phenotypes. We first confirmed by RNA-seq that the

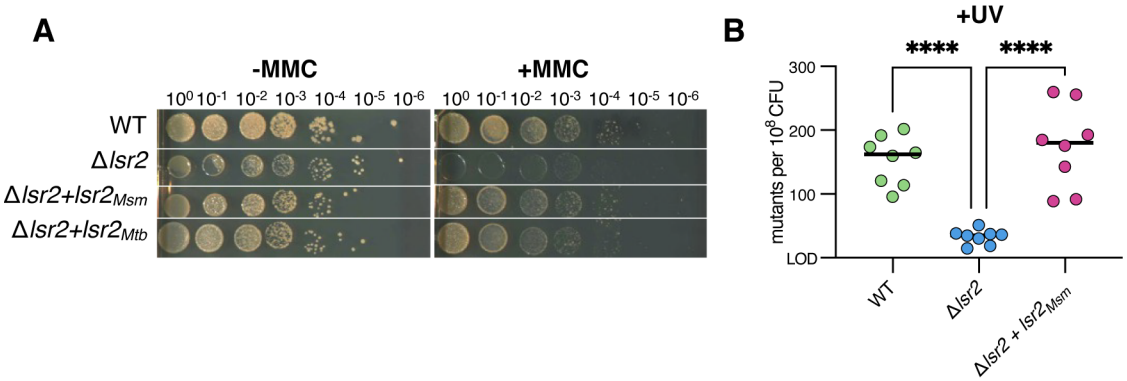

FIGURE 4. Lsr2 mediates survival to mitomycin and UV-induced mutagenesis. (A) Serial dilutions of WT, Δ*lsr2*, and complemented strains on agar plates with or without mitomycin C (1.56 ng/ml). Results shown are representative spots of biological triplicates (**Fig. S5**). **(D)** Frequency of rifampin-resistant mutants per 10^8 cfu with UV-induced DNA damage (20 mJ/cm^2). LOD refers to the limit of detection. *lsr2* complements were expressed from the native *lsr2* promoter on a phage integrative plasmid. p-values were obtained by one-way ANOVA (****), p<0.0001.

200 expression of mutasome components or other genes related to the DNA-damage response was
201 unaltered in Δ*lsr2* (**Supplementary Tables 1-9**). Then, to test our model, we grew cells on agar
202 plates with different concentrations of MMC. Deletion of *lsr2* results in a severe growth defect in
203 the presence of MMC, which could be complemented by the expression of *lsr2* from *M.*
204 *smegmatis* or *M. tuberculosis* (**Fig. 4A, Fig. S5**). Next, we assayed the ability of Δ*lsr2* to
205 acquire resistance to rifampicin when exposed to UV. We chose a dose of UV that resulted in
206 no survival difference between the two genotypes (**Fig. S6**). Consistent with a role in DNA
207 damage response, we found that cells deleted for *lsr2* are approximately 4-5 times less likely to
208 acquire resistance to rifampicin when exposed to UV (**Fig. 4B**). Together, our data show that
209 Lsr2 is involved in the exchange of polymerase at the replication fork in both standard culture
210 medium and in conditions that damage DNA and up-regulate repair pathways.

211

212 **DISCUSSION**

213 Lsr2 acts as a transcriptional repressor for many genes on the *M. smegmatis* and *M.*
214 *tuberculosis* chromosomes (17, 22-24). Additionally, multiple lines of evidence suggest that Lsr2
215 has other roles aside from its function as a transcription factor (22, 25, 26). Our results implicate
216 Lsr2 as a potential factor in mycobacterial mutagenesis and antibiotic resistance (**Fig. 6**).

217 While Lsr2 binds to and/or alters the transcription of many genes in both *M. smegmatis*
218 and *M. tuberculosis,* very few phenotypes associated with the deletion mutant have been
219 connected to altered expression of target genes (17, 22, 24). One of the few exceptions is the
220 change in colony morphology, which can be attributed to the increased expression of a putative
221 polyketide synthase (MSMEG_4727) in *M. smegmatis* (24, 30). Why, then, is Lsr2 associated

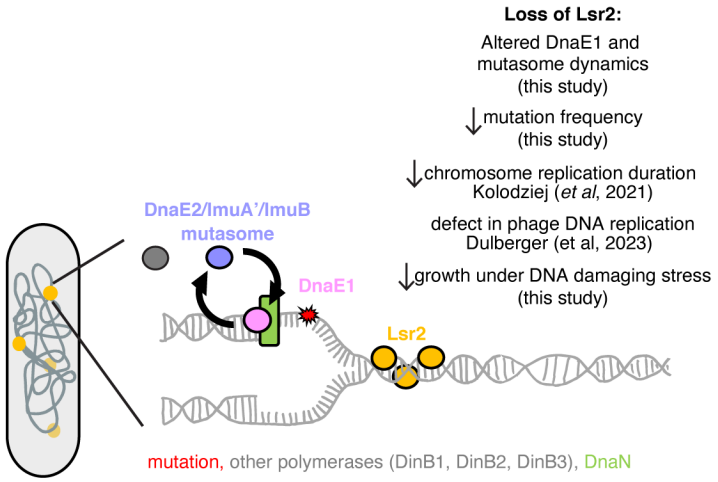

FIGURE 6. Model of Lsr2 regulation of DNA replication and mutagenesis. Our data suggest that loss of *lsr2* results in a decrease in mutagenesis due to a novel role for Lsr2 in modulating replisome dynamics. Specifically, our data are consistent with a model in which Lsr2 acts as a roadblock on the DNA to promote the exchange of the major replicative polymerase DnaE1 with others in the cytoplasmic pool. In conditions that do not induce DNA damage, these polymerases may include DinB1, which contributes to spontaneous mutagenesis (12). In conditions that damage DNA, the mutasome, which is comprised of DnaE2 and its accessory proteins (ImuA' and ImuB), is induced and needs to exchange with the replicative polymerase to repair lesions (13, 18, 19). Deletion of Lsr2 reduces the flexibility of the replisome needed for sufficient exchange, thereby resulting in cells that are more reliant on DnaE1, a higher fidelity polymerase that is unable to bypass lesions. Thus, cells missing *lsr2* are impaired in their ability to grow in conditions that damage DNA in their ability to acquire mutations.

222 with so many bacterial behaviors, including bacterial growth, the cell cycle, robust infection,
223 survival to hydrogen peroxide and antibiotics, survival in low oxygen, and resistance to phage?

224 Our results indicate that one of Lsr2's functions in the cell is to promote the flexibility of
225 the mycobacterial replisome, enabling specialist polymerases like the DnaE2 translesion
226 complex (ImuB/DnaE2/ImuA') to access the replication fork, leading to efficient, but error-prone,
227 DNA replication and cell growth in conditions that damage DNA. Specifically, our findings
228 support a model whereby in non-DNA damaging conditions, Lsr2 serves as an obstacle that
229 promotes the frequent exchange of DnaE1, allowing other polymerases to exchange into the

230 replisome (**Fig. 6**). This model is consistent with *ΔlsR2* having a slightly reduced basal mutation
231 rate, as Lsr2 could be allowing exchange of polymerases besides DnaE1 at a low frequency.
232 Likewise, in DNA damaging conditions, out data suggest a model in which Lsr2-mediated
233 exchange of DnaE1 promotes loading of ImuB and thus DnaE2 and ImuA'. DnaE1 is a more
234 faithful enzyme but is unable to bypass lesions; thus, cells missing *lsr2* grow more slowly under
235 conditions that damage DNA but replicate with higher fidelity.

236 Numerous studies in eukaryotes and other bacteria show that the rate of replication fork
237 progression is actively regulated, in some cases by machinery that slow down DNA replication,
238 to ensure coordination amongst DNA replication, DNA repair, and transcription (31-34). We
239 hypothesize that Lsr2 may function to regulate replication fork progression in mycobacteria, and
240 that this function may provide a unifying explanation for many of the phenotypes associated with
241 loss of *lsr2,* including slower DNA replication in the host and other environmental conditions
242 likely to assault DNA. Likewise, in conditions that do not significantly damage DNA, like those
243 found in laboratory growth media, loss of *lsr2* leads to faster and higher fidelity chromosomal
244 replication, possibly explaining the emergence of spontaneous *lsr2* mutants in several
245 laboratories (30, 35, 36). Additionally, loss of *lsr2* is associated with increased resistance
246 against infection by certain phages, and fewer and smaller zones of phage DNA replication (26).
247 We speculate that efficient turnover of the bacterial host DNA replication machinery mediated by
248 Lsr2 could be required for robust replication of phage DNA and productive infection.

249 Intriguingly, Lsr2 is phosphorylated by PknB, a plasma membrane-bound eukaryotic
250 serine/threonine kinase involved in cell growth and division (37). Future research is needed but
251 we speculate that such regulation could be used to coordinate cell wall synthesis and DNA
252 synthesis during environmental changes or even during a typical cell cycle.

253 Lsr2 may be a promising drug target for preventing the emergence of antibiotic
254 resistance in mycobacteria. Our work adds to the growing body of evidence Lsr2 is at the nexus

255 of several evolutionary tradeoffs, including fast chromosome replication, mutagenesis,
256 replisome flexibility, and phage resistance. Indeed, loss of Lsr2 results in severe growth defects
257 in *M. tuberculosis* and *M. abscessus in vivo* (20, 23). Thus, we speculate that targeting Lsr2
258 therapeutically may help treat drug-susceptible infections, while preventing the emergence of
259 drug resistance.

260

261
262 **MATERIALS AND METHODS**

263 **Strains and growth conditions**

264 All mycobacterial strains are derivatives of *Mycobacterium smegmatis* MC2 155. Cells were
265 grown in Middlebrook 7H9 broth supplemented with 0.05% (v/v) Tween80, ADC, and 0.2% (v/v)
266 glycerol for liquid culture. LB agar was used as solid media. Liquid cultures were grown at 37 °C
267 on a rotator. Agar plates were incubated at 37 °C. If applicable, antibiotics were added at the
268 following final concentrations: hygromycin B (50 ug/mL), kanamycin (25ug/mL), nourseothricin
269 (20 ug/ml), zeocin (20 ug/mL), and gentamicin (5 ug/ml).

270 Plasmid DNA for transformation into *M. smegmatis* was prepared from *E. coli* (DH5a,
271 XL1). If applicable, antibiotics were added at the following final concentrations: hygromycin B
272 (100 ug/mL), kanamycin (50 ug/mL), and nourseothricin (40 ug/ml). Plasmid constructs were
273 generated using Gibson cloning and phage-based integrative vectors. Fluorescent protein
274 fusions were generated using mGFPmut3 and mScarlet-I variants.

275 Genetic modifications to the native locus were generated as previously described using
276 the mycobacterial Che9c phage RecET recombination system (38). To construct a knockout, we
277 designed a dsDNA substrate encoding a zeocin resistance cassette flanked by loxP sites and
278 ~500bp of homology on either end of the locus of interest. The dsDNA substrate was then
279 electroporated into *M. smegmatis* strains carrying a plasmid encoding isovaleronitrile-inducible
280 expression of RecET. Colonies were selected by zeocin resistance and screened by PCR using
281 primers annealing to regions flanking dsDNA insertion. In some cases, the zeocin resistance
282 cassette was removed by Cre-Lox recombination. Strains and primers are listed in Tables S12
283 and S13, respectively.

284

285 **Fluorescence microscopy**

286 All microscopy experiments were performed on a Nikon TI-E inverted wide-field microscope
287 equipped with the Nikon Perfect Focus System, an ORCA-Flash4.0 Digital CMOS Camera
288 (Hamamatsu) and an environmental control chamber maintained at 37 °C.
289
290 **Time-lapse and kymograph analysis:** Time-lapse imaging was done using a 60X Oil 1.45NA
291 Plan Apochromat phase-contrast objective. Bacterial samples were loaded and grown in a B04A
292 microfluidic plate (CellAsic ONIX, B04A-03-5PK). Phase and fluorescence images were
293 acquired every 30 minutes using NIS Elements software. Fluorescence images were taken
294 sequentially using a 470 nm excitation laser and 515/30 emission filter for msfGFP and
295 mGFPmut3, and a 555 nm excitation laser and a 595/40 emission filter for mScarletI.
296 Kymograph analysis was performed using a custom pipeline for segmenting and tracking
297 cells, and extracting fluorescence profiles. Cell segmentation was performed on the phase
298 image using a U-Net network trained for segmenting mycobacterial cells (39). Semi-automated
299 cell tracking and extraction of fluorescence profiles from background-subtracted images was
300 done using a custom MATLAB program and open-source image analysis software Fiji (40).
301 Average kymographs were generated by 2D interpolation of at least twenty individual
302 kymographs.
303
304 **FRAP:** FRAP experiments were done using a 60X oil DIC objective. Bacterial cells were imaged
305 under 7H9 agar pads (1% agar, 0.2% (v/v) glycerol) in 50 mm glass-bottomed dishes.
306 Fluorescent spots were manually selected for localized bleaching with a focused 405-nm laser.
307 Two pre-bleach fluorescence images were acquired: one to identify and center a target focus,
308 and a second for quantification of total pre-bleach fluorescence. Fluorescence recovery was
309 monitored by acquisition at pre-defined intervals (2 to 10 sec) following photobleaching using an
310 exposure time of 200 ms.

311 Cell outlines for determination of total pre-bleach fluorescence were manually drawn
312 using the brightfield image. Fluorescence images were background subtracted and corrected for
313 photobleaching. To quantify the fluorescence of bleached foci over time, a circular ROI was
314 manually drawn around the bleached foci and intensity profiles over time were obtained using
315 Fiji (40). Fluorescence recovery curves were generated by first normalizing fluorescence
316 intensity profiles to pre-bleach focus fluorescence. The post-bleach value was then subtracted
317 from all time points. Maximum recovery was estimated by calculating the total amount of
318 fluorescence in the cell after photobleaching outside the focus. Finally, all time points were
319 divided by the estimated maximum recovery value, such that a value of 0 and 1 correspond to
320 no recovery and maximum recovery, respectively.
321
322 **RNA-seq of WT *M. smegmatis* and Δ*lsr2***
323 WT *M. smegmatis* and Δ*lsr2* were grown in triplicate at 37°C to OD600 ~0.7-1.0. For mitomycin
324 treatment, 1 ml of cells were added to 4 ml of 7H9 containing 100 ng/ml mitomycin C for a final
325 concentration of 80 ng/ml mitomycin C. Approximately 2-4 ml of cells were harvested at each
326 timepoint and incubated with 2 volumes of RNAprotect (Qiagen) at room temperature for 5
327 minutes prior to centrifugation for 5 minutes at 4000xg 4°C. The supernatant was discarded,
328 and the cells were then immediately used for RNA extraction or stored at -80°C.
329 RNA extraction was performed using the Qiagen RNeasy Kit (74104). Cells were
330 resuspended in 500 ul of RLT buffer (Qiagen) with 2-mercaptoethanol and homogenized by
331 bead beating for 3 minute pulses at maximum speed, three times, with 5 minutes of rest on ice
332 in-between. The lysate was then centrifuged at maximum speed for 1 minute, and the
333 supernatant was transferred to a new tube. The remainder of the RNA extraction was performed
334 using the Qiagen RNeasy Kit according to manufacturer instructions. RNA quality was verified
335 using a bioanalyzer (Agilent Technologies TapeStation 2200). DNase treatment and ribosomal

336 RNA depletion were performed at the Microbial Genome Sequencing Center before library
337 preparation and sequencing.
338
339 **Mutation frequency analysis**
340 10 ml of bacterial cells were grown to OD600 ~0.7-1.0. 5 ml of cells were UV irradiated (20
341 mJ/cm2 UV; Stratalinker UV crosslinker), while the remaining 5 ml of cells were used for the
342 untreated control. Treated and untreated samples were then added to an equal volume of fresh
343 7H9 media and outgrown for 3 hours at 37°C. 100 ul liquid culture was used for CFU
344 determination, and the remainder of the culture was plated onto Rif-containing LB agar plates
345 (200 ug/ml) for mutant detection. All mutation frequency measurements were performed using 8
346 biological replicates. Rif-resistant colonies were enumerated after 5-7 days of incubation at
347 37°C. CFU plates were read after about 2-3 days of growth on non-selective media. Mutation
348 frequencies were calculated by the number of Rif-resistant colonies per ml of culture by the
349 CFU/ml.
350
351 **Spot assay**
352 Bacterial cells were grown to OD600 ~0.7-1.0, normalized to the same OD, and then 10-fold
353 serially diluted. 5 ul of culture were spotted on LB agar containing varying concentrations of
354 antibiotic. Plates were imaged after incubation at 37°C for 2-3 days. All assays were done in
355 biological triplicate.
356
357 **RESOURCE AVAILABILITY**
358 **Lead contact**

Further information and requests for resources and reagents should be directed to and will be fulfilled by the lead contact, Dr. Hesper Rego (hesper.rego@yale.edu).

Materials availability

All unique/stable reagents generated in this study are available from the lead contact.

Data availability

RNA-seq sequencing data are deposited to the Short Read Archive (SRA) under project number: PRJNA1060683

ACKNOWLEDGMENTS

We thank members of the Rego lab for helpful suggestions, and Dr. Eduardo Groisman for discussions. This work was supported by NIH R01 AI148255 and the Searle and Pew Foundations to EHR.

AUTHOR CONTRIBUTIONS

WLN and EHR conceived experiments and analyzed data. WLN performed experiments. WLN and EHR wrote the manuscript. EHR secured funding for the work.

TABLES S1-6. All quantified RNA-seq read counts for WT and Δ*lsr2*, in triplicate, treated with mitomycin-C at 0, 1, 3, 6, or 24 hours.
*see attached

TABLES S7-11. Differentially expressed genes in WT and Δ*lsr2* treated with mitomycin-C 0, 1, 3, 6, or 24 hours
*see attached

386 **TABLE S12.** Strain list

STRAIN	GENOTYPE	SOURCE	Additional information
WN788	mc2155Δlsr2::zeoR	This work	*lsr2* deletion strain
WN906	mc2155Δlsr2::zeoR L5::plsr2-mScarletI-FLAG Giles::pimuAB-msfGFP-myc Tweety::pNative-MSMEG6092	This work	*lsr2* deletion strain, complemented with untagged *M. smegmatis* Lsr2
WN874	mc2155Δlsr2::zeoR Giles::pimuAB-msfGFP-myc Tw::pdnaE2-mScarletI-FLAG L5::pNative-Rv3597c	This work	*lsr2* deletion strain, complemented with untagged *M. tuberculosis* Lsr2
WN1384	mc2155 Giles::pNative-dnae1-mScarletI-FLAG	This work	C-terminal DnaE1 fusion in a WT background
WN1385	mc2155Δlsr2::zeoR Giles::pNative-dnae1-mScarletI-FLAG	This work	C-terminal DnaE1 fusion in a Δ*lsr2* background
WN1390	mc2155Δlsr2::zeoR L5::pNative-MSMEG6092-mScarletI-FLAG Giles::pTetO-DnaE1-mGFPmut3-myc	This work	Dual-labeled C-terminal Lsr2 and C-terminal DnaE1 fusions in a Δ*lsr2* background
WN573	mc2155ΔimuAB::loxP	This work	*imuAB* deletion strain
WN1278	mc2155ΔimuAB::loxP L5::pJR962-LexA sgRNA Giles::pNative-imuA_FLAG-mScarletI-imuB-1550DS	This work	Translational fusion of ImuB
WN1280	mc2155Δimuab::loxP Δlsr2::zeoR L5::pJR962-LexA sgRNA Giles::pNative-imuA_FLAG-mScarletI-imuB-1550DS	This work	Translational fusion of ImuB in Δ*lsr2* background
WN1318	mc2155Δimuab::loxP L5::pJR962-LexA sgRNA Giles::pNative-imuA-mScarletI-FLAG_imuB-1550DS	This work	Translational fusion of ImuA'
WN273	mc2155Δdnae2::zeoR	This work	*dnaE2* deletion strain
WN171	mc2155 rpoB::mApple-hygR dnaE2:: mGFPmut3-zeoR	This work	Translational fusion of DnaE2

387

388

TABLE S11. Primer list

*see attached

References

1. Fuchs RP, Fujii S. 2013. Translesion DNA synthesis and mutagenesis in prokaryotes. Cold Spring Harb Perspect Biol 5:a012682.
2. Galagan JE. 2014. Genomic insights into tuberculosis. Nature Reviews Genetics 15:307-320.
3. Boritsch EC, Khanna V, Pawlik A, Honoré N, Navas VH, Ma L, Bouchier C, Seemann T, Supply P, Stinear TP, Brosch R. 2016. Key experimental evidence of chromosomal DNA transfer among selected tuberculosis-causing mycobacteria. Proceedings of the National Academy of Sciences 113:9876-9881.
4. Rock JM, Lang UF, Chase MR, Ford CB, Gerrick ER, Gawande R, Coscolla M, Gagneux S, Fortune SM, Lamers MH. 2015. DNA replication fidelity in Mycobacterium tuberculosis is mediated by an ancestral prokaryotic proofreader. Nat Genet 47:677-81.
5. Dupuy P, Ghosh S, Adefisayo O, Buglino J, Shuman S, Glickman MS. 2022. Distinctive roles of translesion polymerases DinB1 and DnaE2 in diversification of the mycobacterial genome through substitution and frameshift mutagenesis. Nature Communications 13:4493.
6. Boshoff HI, Reed MB, Barry CE, 3rd, Mizrahi V. 2003. DnaE2 polymerase contributes to in vivo survival and the emergence of drug resistance in Mycobacterium tuberculosis. Cell 113:183-93.
7. Dupuy P, Ghosh S, Fay A, Adefisayo O, Gupta R, Shuman S, Glickman MS. 2023. Roles for mycobacterial DinB2 in frameshift and substitution mutagenesis. Elife 12.
8. Kana BD, Abrahams GL, Sung N, Warner DF, Gordhan BG, Machowski EE, Tsenova L, Sacchettini JC, Stoker NG, Kaplan G, Mizrahi V. 2010. Role of the DinB homologs Rv1537 and Rv3056 in Mycobacterium tuberculosis. J Bacteriol 192:2220-7.
9. Ordonez H, Shuman S. 2014. Mycobacterium smegmatis DinB2 misincorporates deoxyribonucleotides and ribonucleotides during templated synthesis and lesion bypass. Nucleic Acids Res 42:12722-34.
10. Ordonez H, Uson ML, Shuman S. 2014. Characterization of three mycobacterial DinB (DNA polymerase IV) paralogs highlights DinB2 as naturally adept at ribonucleotide incorporation. Nucleic Acids Res 42:11056-70.
11. Warner DF, Ndwandwe DE, Abrahams GL, Kana BD, Machowski EE, Venclovas Č, Mizrahi V. 2010. Essential roles for imuA′- and imuB-encoded accessory factors in DnaE2-dependent mutagenesis in Mycobacterium tuberculosis. Proceedings of the National Academy of Sciences 107:13093-13098.
12. Joseph AM, Badrinarayanan A. 2020. Visualizing mutagenic repair: novel insights into bacterial translesion synthesis. FEMS Microbiol Rev 44:572-582.
13. Beattie TR, Kapadia N, Nicolas E, Uphoff S, Wollman AJ, Leake MC, Reyes-Lamothe R. 2017. Frequent exchange of the DNA polymerase during bacterial chromosome replication. Elife 6.
14. Logsdon MM, Ho PY, Papavinasasundaram K, Richardson K, Cokol M, Sassetti CM, Amir A, Aldridge BB. 2017. A Parallel Adder Coordinates Mycobacterial Cell-Cycle Progression and Cell-Size Homeostasis in the Context of Asymmetric Growth and Organization. Curr Biol 27:3367-3374.e7.
15. Helmstetter CE, Cooper S. 1968. DNA synthesis during the division cycle of rapidly growing Escherichia coli Br. Journal of Molecular Biology 31:507-518.

16. Trojanowski D, Kołodziej M, Hołówka J, Müller R, Zakrzewska-Czerwińska J. 2019. Watching DNA Replication Inhibitors in Action: Exploiting Time-Lapse Microfluidic Microscopy as a Tool for Target-Drug Interaction Studies in Mycobacterium. Antimicrob Agents Chemother 63.
17. Colangeli R, Helb D, Vilchèze C, Hazbón MH, Lee CG, Safi H, Sayers B, Sardone I, Jones MB, Fleischmann RD, Peterson SN, Jacobs WR, Jr., Alland D. 2007. Transcriptional regulation of multi-drug tolerance and antibiotic-induced responses by the histone-like protein Lsr2 in M. tuberculosis. PLoS Pathog 3:e87.
18. Gordon BR, Imperial R, Wang L, Navarre WW, Liu J. 2008. Lsr2 of Mycobacterium represents a novel class of H-NS-like proteins. J Bacteriol 190:7052-9.
19. Gehrke EJ, Zhang X, Pimentel-Elardo SM, Johnson AR, Rees CA, Jones SE, Hindra, Gehrke SS, Turvey S, Boursalie S, Hill JE, Carlson EE, Nodwell JR, Elliot MA. 2019. Silencing cryptic specialized metabolism in Streptomyces by the nucleoid-associated protein Lsr2. eLife 8:e47691.
20. Le Moigne V, Bernut A, Cortès M, Viljoen A, Dupont C, Pawlik A, Gaillard JL, Misguich F, Crémazy F, Kremer L, Herrmann JL. 2019. Lsr2 Is an Important Determinant of Intracellular Growth and Virulence in Mycobacterium abscessus. Front Microbiol 10:905.
21. Wiechert J, Filipchyk A, Hünnefeld M, Gätgens C, Brehm J, Heermann R, Frunzke J. 2020. Deciphering the Rules Underlying Xenogeneic Silencing and Counter-Silencing of Lsr2-like Proteins Using CgpS of Corynebacterium glutamicum as a Model. mBio 11.
22. Colangeli R, Haq A, Arcus VL, Summers E, Magliozzo RS, McBride A, Mitra AK, Radjainia M, Khajo A, Jacobs WR, Salgame P, Alland D. 2009. The multifunctional histone-like protein Lsr2 protects mycobacteria against reactive oxygen intermediates. Proceedings of the National Academy of Sciences 106:4414-4418.
23. Bartek IL, Woolhiser LK, Baughn AD, Basaraba RJ, Jacobs WR, Jr., Lenaerts AJ, Voskuil MI. 2014. Mycobacterium tuberculosis Lsr2 is a global transcriptional regulator required for adaptation to changing oxygen levels and virulence. mBio 5:e01106-14.
24. Kołodziej M, Łebkowski T, Płociński P, Hołówka J, Paściak M, Wojtaś B, Bury K, Konieczny I, Dziadek J, Zakrzewska-Czerwińska J. 2021. Lsr2 and Its Novel Paralogue Mediate the Adjustment of Mycobacterium smegmatis to Unfavorable Environmental Conditions. mSphere 6.
25. Kołodziej M, Trojanowski D, Bury K, Hołówka J, Matysik W, Kąkolewska H, Feddersen H, Giacomelli G, Konieczny I, Bramkamp M, Zakrzewska-Czerwińska J. 2021. Lsr2, a nucleoid-associated protein influencing mycobacterial cell cycle. Scientific Reports 11:2910.
26. Dulberger CL, Guerrero-Bustamante CA, Owen SV, Wilson S, Wuo MG, Garlena RA, Serpa LA, Russell DA, Zhu J, Braunecker BJ, Squyres GR, Baym M, Kiessling LL, Garner EC, Rubin EJ, Hatfull GF. 2023. Mycobacterial nucleoid-associated protein Lsr2 is required for productive mycobacteriophage infection. Nature Microbiology 8:695-710.
27. Gessner S, Martin ZA-M, Reiche MA, Santos JA, Dinkele R, Ramudzuli A, Dhar N, de Wet TJ, Anoosheh S, Lang DM, Aaron J, Chew T-L, Herrmann J, Müller R, McKinney JD, Woodgate R, Mizrahi V, Venclovas Č, Lamers MH, Warner DF. 2023. Investigating the composition and recruitment of the mycobacterial ImuA′–ImuB–DnaE2 mutasome. eLife 12:e75628.
28. Santos JA, Timinskas K, Lamers MH, Venclovas Č, Warner DF, Gessner SJ. 2023. RecA-NT homology motif in ImuB is essential for mycobacterial ImuA'-ImuB protein interaction and mutasome function. bioRxiv doi:10.1101/2023.03.28.534377.
29. Goodman MF, McDonald JP, Jaszczur MM, Woodgate R. 2016. Insights into the complex levels of regulation imposed on Escherichia coli DNA polymerase V. DNA Repair (Amst) 44:42-50.

30. Báez-Ramírez E, Querales L, Aranaga CA, López G, Guerrero E, Kremer L, Carrère-Kremer S, Viljoen A, Daffé M, Laval F, Cole ST, Benjak A, Alzari P, André-Leroux G, Jacobs WR, Vilcheze C, Takiff HE. 2021. Elimination of PknL and MSMEG_4242 in Mycobacterium smegmatis alters the character of the outer cell envelope and selects for mutations in Lsr2. The Cell Surface 7:100060.
31. Tan KW, Pham TM, Furukohri A, Maki H, Akiyama MT. 2015. Recombinase and translesion DNA polymerase decrease the speed of replication fork progression during the DNA damage response in Escherichia coli cells. Nucleic Acids Res 43:1714-25.
32. Munden A, Rong Z, Sun A, Gangula R, Mallal S, Nordman JT. 2018. Rif1 inhibits replication fork progression and controls DNA copy number in Drosophila. eLife 7:e39140.
33. Kobayashi T, Horiuchi T. 1996. A yeast gene product, Fob1 protein, required for both replication fork blocking and recombinational hotspot activities. Genes Cells 1:465-74.
34. Tsirkas I, Dovrat D, Thangaraj M, Brouwer I, Cohen A, Paleiov Z, Meijler Michael M, Lenstra T, Aharoni A. 2022. Transcription-replication coordination revealed in single live cells. Nucleic Acids Research 50:2143-2156.
35. Arora K, Whiteford DC, Lau-Bonilla D, Davitt CM, Dahl JL. 2008. Inactivation of lsr2 results in a hypermotile phenotype in Mycobacterium smegmatis. J Bacteriol 190:4291-300.
36. Kocíncová D, Singh AK, Beretti JL, Ren H, Euphrasie D, Liu J, Daffé M, Etienne G, Reyrat JM. 2008. Spontaneous transposition of IS1096 or ISMsm3 leads to glycopeptidolipid overproduction and affects surface properties in Mycobacterium smegmatis. Tuberculosis (Edinb) 88:390-8.
37. Alqaseer K, Turapov O, Barthe P, Jagatia H, De Visch A, Roumestand C, Wegrzyn M, Bartek IL, Voskuil MI, O'Hare HM, Ajuh P, Bottrill AR, Witney AA, Cohen-Gonsaud M, Waddell SJ, Mukamolova GV. 2019. Protein kinase B controls Mycobacterium tuberculosis growth via phosphorylation of the transcriptional regulator Lsr2 at threonine 112. Mol Microbiol 112:1847-1862.
38. Murphy KC, Papavinasasundaram K, Sassetti CM. 2015. Mycobacterial recombineering. Methods Mol Biol 1285:177-99.
39. Falk T, Mai D, Bensch R, Çiçek Ö, Abdulkadir A, Marrakchi Y, Böhm A, Deubner J, Jäckel Z, Seiwald K, Dovzhenko A, Tietz O, Dal Bosco C, Walsh S, Saltukoglu D, Tay TL, Prinz M, Palme K, Simons M, Diester I, Brox T, Ronneberger O. 2019. U-Net: deep learning for cell counting, detection, and morphometry. Nature Methods 16:67-70.
40. Schindelin J, Arganda-Carreras I, Frise E, Kaynig V, Longair M, Pietzsch T, Preibisch S, Rueden C, Saalfeld S, Schmid B, Tinevez J-Y, White DJ, Hartenstein V, Eliceiri K, Tomancak P, Cardona A. 2012. Fiji: an open-source platform for biological-image analysis. Nature Methods 9:676-682.

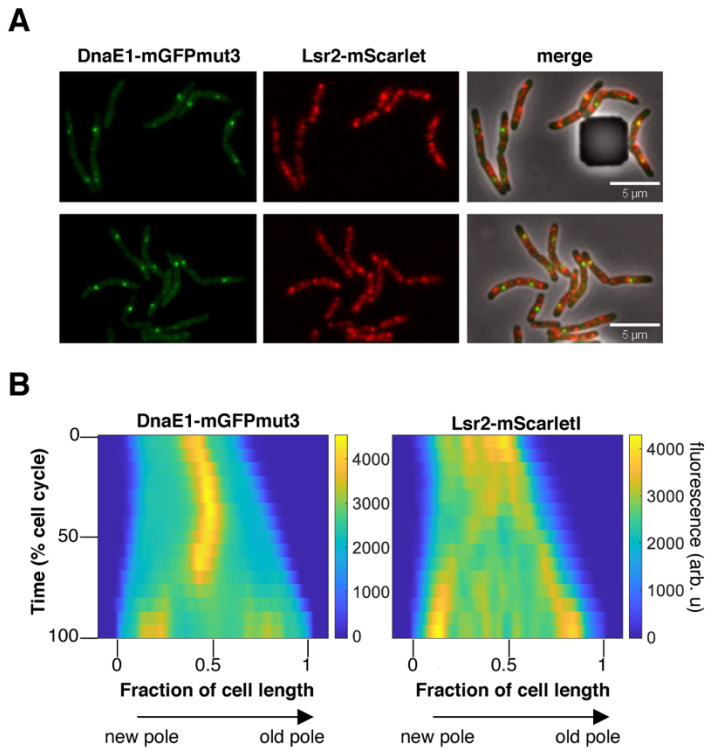

529

530 **Figure S1. DnaE1 and Lsr2 do not co-localize. (A)** Microscopy images of cells expressing

531 DnaE1-mGFPmut3 and Lsr2-mScarlet in Δ*lsr2*. **(B)** Average kymographs for each fusion (N=28

532 cells).

533

534

535

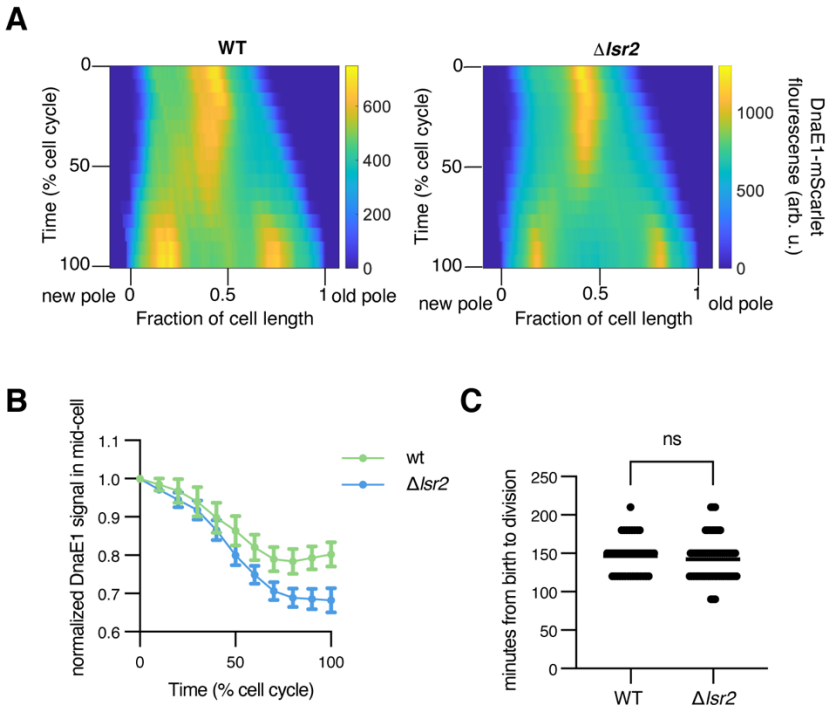

Figure S2. (A) Kymograph of DnaE1-mScarlet expressed from the native promoter on a phage integrative plasmid in WT (left, N=43) or Δ*lsr2* (right, N=59). WT is the same as main text Figure 1B for comparison. **(B)** From the cells shown in panel A, the fluorescence at mid-cell from was normalized to time 0 and plotted over time. **(C)** Time between birth and division as determine by visible invaginations on the phase contrast images was measured for both WT and Δ*lsr2* cells.

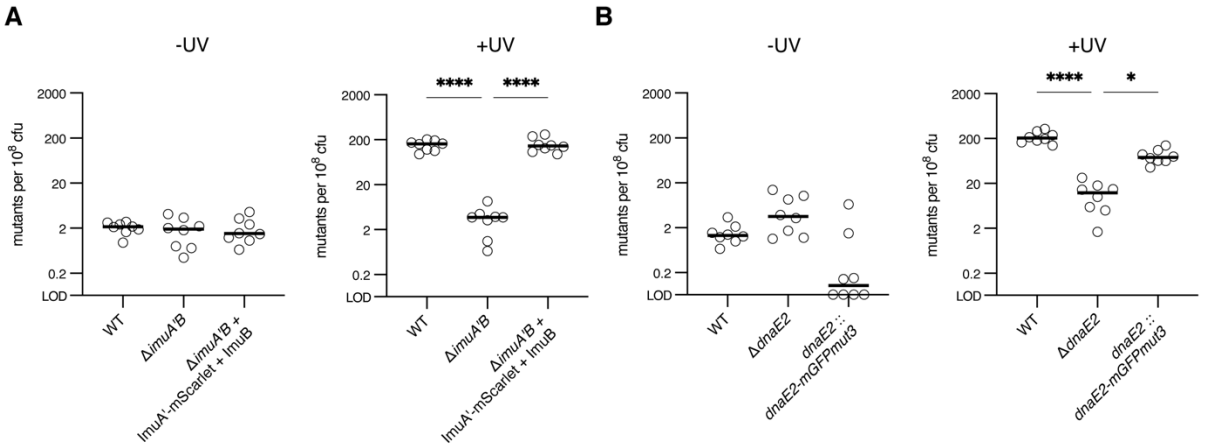

Figure S3. ImuA' and DnaE2 translational fusions maintain functionality in UV-induced mutagenesis. Frequency of rifampin-resistant mutants per 10^8 cfu without or with UV-induced DNA damage (20 mJ/cm^2 UV). **(A)** Results shown are for WT, *imuA'B* deletion, or *imuA'B* deletion complemented with a fluorescent translational fusion of ImuA' and ImuB. **(B)** Results shown are for WT, *dnaE2* deletion, and *dnaE2* deletion complemented with a fluorescent translational fusion of DnaE2. Complements are expressed from the native promoter on a phage integrative plasmid. LOD refers to the limit of detection. p-values were obtained by one-way ANOVA. 0.1234 (ns), 0.0332 (*), 0.0021 (**), 0.0002 (***), <0.0001 (****).

555

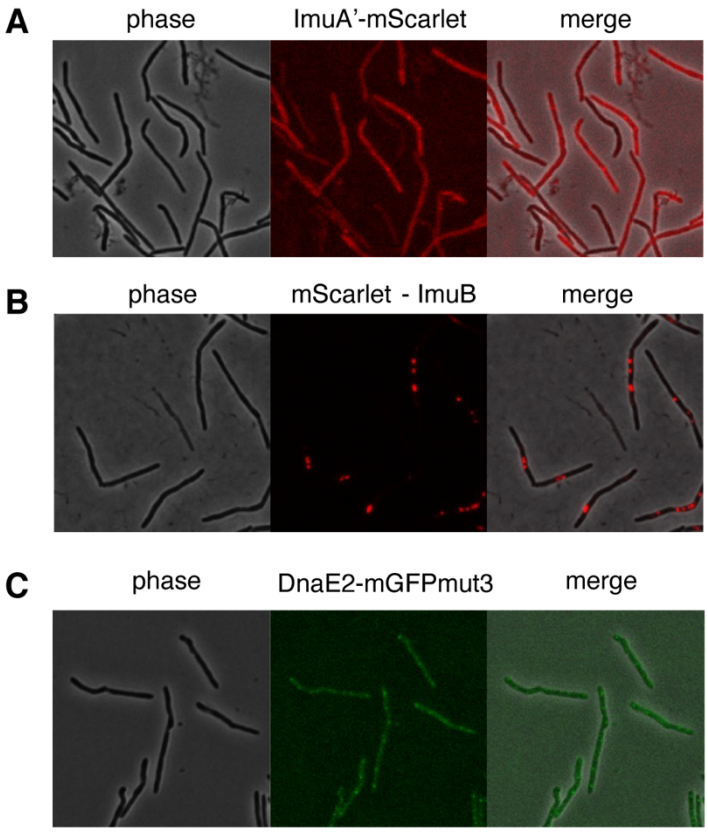

556

557 **Figure S4. Microscopy images of mutasome translational fusions. Images shown are of**
558 **(A)** *imuA'B* deletion mutant complemented with a fluorescent translational fusion of ImuA' and
559 ImuB, **(B)** *imuA'B* deletion mutant complemented with ImuA and a fluorescent translational
560 fusion of ImuB, and **(C)** *dnaE2* deletion mutant complemented with a fluorescent translational
561 fusion of DnaE2. Complements are expressed from the native promoter on a phage integrative
562 plasmid. DNA damage was induced by mitomycin C treatment (80 ng/ml) for 4-6 hours. Images
563 were acquired using 1 second **(A, B)** or 500 ms **(C)** exposure times.

564

565

566

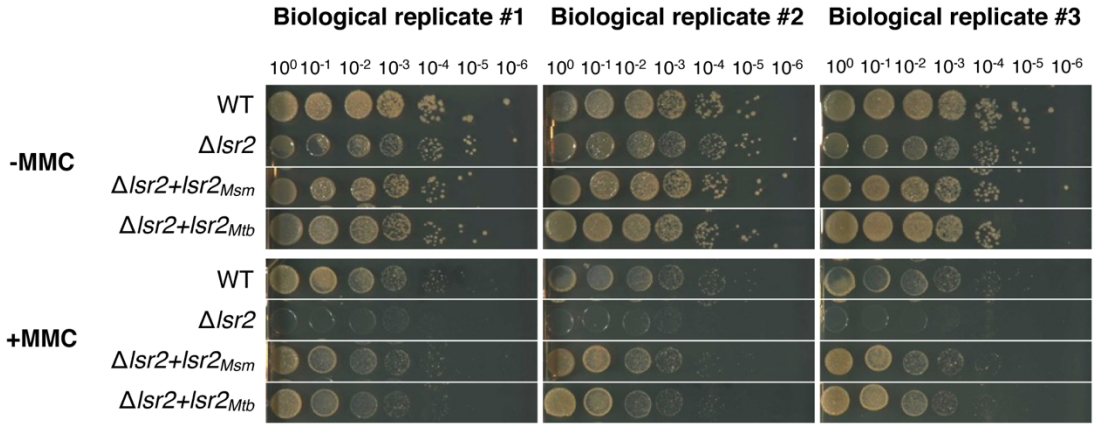

Figure S5. Loss of *lsr2* leads to growth defects on mitomycin C. Serial dilutions of WT, Δ*lsr2*, and complemented strains on agar plates with or without mitomycin C (1.56 ng/ml) in biological triplicate. *M. smegmatis* and *M. tuberculosis lsr2* complements were expressed from the native *lsr2* promoter on a phage integrative plasmid.

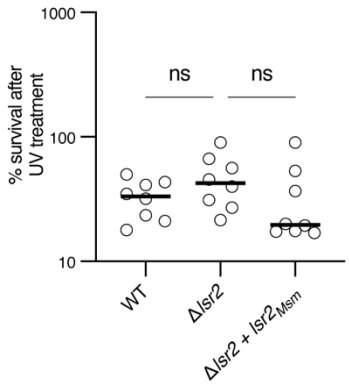

574
575 **Figure S6. Loss of *lsr2* is not associated with a decrease in survival following UV**
576 **treatment.** WT, Δ*lsr2*, and complement, were treated with 20 mJ/cm^2 UV and plated for cfu.
577 Percent survival is the ratio of cfu/ml for UV-treated cells divided by the cfu/ml for untreated cells
578 multiplied by 100. p-values were obtained by one-way ANOVA. 0.1234 (ns), 0.0332 (*), 0.0021
579 (**), 0.0002 (***), <0.0001 (****).

580

581

582